5.1 Introduction

In previous chapter, we reported an anomalous increase in T_N from120 K to ~350K on reducing the size from 120 nm to 18 nm in the tetragonal phase of (1-x)$BiFeO_3$-x$PbTiO_3$solid solution for x=0.50.The tetragonal phase of BF-xPT is unusual because of its large tetragonality (η= (c/a -1) that affects the superexchange interactions also. For example, the T_N of the monoclinic phase of BF-xPT with x=0.27is ~473K which suddenly drops to ~ 210Kfor x=0.31 as a result of the morphotropic structural phase transition to the tetragonal phase in the bulk samples [Bhattacharjee et al. (2010)].This is quite intriguing. Had this drop been due to due to slight increase (4%) in disorder content of the magnetic sublattice, the T_N should have been ~ 453K, being the extrapolated value of T_N from the monoclinic side. It was argued that the low value of T_N of bulk tetragonal compositions across the MPB is due to the large ferroelectric distortion (η=c/a-1) caused by the off centering of Fe^{3+}/Ti^{4+} ions in the oxygen octahedral environment that breaks the covalent bond, and hence the superexchange interaction pathway, along the [001] direction reducing the dimensionality of the AFM state to d= 2 (ie, 2d-AFM) [Bhattacharjee et al. (2010), Yashima et al. (2011)]. More significantly, it was demonstrated that the anomalous increase in T_N on decreasing the particle size of the tetragonal compositions is linked with the crossover from nearly 2d AFM ordering in bulk to a 3d AFM ordering in smaller particles due to reestablishment of superexchange interactions in the [001] direction as a result of reduced ferroelectric distortion in the tetragonal structure[chapter IV].Thus the anomalous increase in T_N with decreasing size is a consequence of the complex interplay between ferroelectric distortion and the strength of the superexchange interactions both of which can be modulated through size.

As mentioned earlier, the structure of BF-xPT changes from tetragonal (space group P4mm) for $x \geq 0.31$ to monoclinic (space group Cc) for $x \leq 0.27$ while the two phases coexist in the morphotropic phase boundary (MPB) region [Bhattacharjee et al (2007)].The nature of 3d AFM ordering in the pseudorhombohedral monoclinic phase of BF-xPT is similar to the 3d AFM phase of pure BF, except for the fact that PT substitution leads to the lowering of the space group symmetry from R3c to Cc[Bhattacharjee et al.(2010)].It is of interest to investigate the effect of particle size in such monoclinic compositions also to understand the role of ferroelectric distortion on the T_N. We show here that unlike pure BF, where T_N decreases with decreasing particle size as per the predictions of the scaling theories, the T_N of the monoclinic phase of BF-xPT in fact increases with decreasing particle size [Binder (1972)].Our findings highlight an ignored facet of magnetoelectric coupling in multiferroics in the literature where by ferroelectric distortion and its manipulation through particle size can be used to tailor the strength of the magnetic interactions and hence the magnetic transition temperatures. We present the results of high resolution synchrotron x-ray diffraction (SXRD), neutron powder diffraction (NPD) and magnetization measurements on both bulk and nanocrystalline powders of a pseudorhombohedral monoclinic composition of BF-xPT with $x=0.25$ to illustrate the anomalous size effect.

5.2 Experimental

Powders of BF-0.25PT solid solution with different sizes were synthesized using sol-gel technique the details of which are given in chapter II. X-ray diffraction (SXRD) patterns were also recorded at high resolution powder diffraction beamline P02.2 at PETRAIII, DESY, Hamburg, Germany for resolving the controversy about the true space group symmetry (R3c or Cc) of BF-0.25PT discussed in chapter III.

Magnetic measurements at and above room temperature were carried out using a Quantum Design Evercool MPMS3 with a high temperature attachment capable of going up to 1000 K. Temperature dependent magnetization M(T) measurements were carried out on zero field cooled samples while heating under a magnetic field of 500 Oe. Magnetization (M) vs applied field (H) hysteresis measurements were also performed at different temperatures up to a field of 5 Tesla.

Neutron powder diffraction (NPD) patterns were recorded on the high-resolution powder thermal neutron diffractometer HRPT at the Swiss Spallation Neutron Source (SINQ) at Paul Scherrer Institute, Switzerland. The neutron beam with a wavelength of 1.494 Å obtained by using a (533) refection from a vertically focusing Ge-monochromator was used. The diffraction signal was recorded using a position-sensitive detector in the 2θ range of 5 and 165^0.

Rietveld refinements were carried out using FULLPROF package [Carvajal (1993)]. For refining the magnetic structure, Rietveld refinements were carried out using the FULLPROF packageand BasIrreps software in the same package.

5.3 Rietveld analysis of the neutron powder diffraction pattern

As far as the magnetic structure of BF-0.25PT is concerned, there is only one magnetically active cation, $Fe^{3+,}$ in this solid solution, and the magnetic structure therefore corresponds to the arrangement of magnetic moments of Fe^{3+} sublattice only.

Since the Cc space group of BF-0.25PT already possesses a doubled perovskite cell, the magnetic structure can be represented by the propagation vector k = (0,0,0). The magnetic representation of the Fe sublattice (4a Wyckoff site) can be decomposed into two irreducible representations (IRs), each having three basis vectors, as, $\Gamma^{4a} = 3[\Gamma^{1} + \Gamma^{2}]$, leading to two possible configurations of the magnetic moments in the monoclinic phase:

$$\Gamma_1: G^X=S_1^X-S_2^X+S_3^X-S_4^X,\ F^Y= S_1^Y+S_2^Y+S_3^Y+S_4^Y,\ G^Z= S_1^Z-S_2^Z+S_3^Z-S_4^Z$$

$$\Gamma_2: F^X=S_1^X+S_2^X+S_3^X+S_4^X,\ G^Y= S_1^Y-S_2^Y+S_3^Y-S_4^Y,\ F^Z=S_1^Z+S_2^Z+S_3^Z+S_4^Z$$

where, the symbols F and G stand for ferromagnetic and G-type antiferromagnetic arrangements of moments (Bertaut's notation [Bertaut (1968)]) while Si (i=1 to 4) stand for the components of the ith atomic site. The superscripts X, Y, and Z in G, F and Si represent the [100], [010] and [001] directions of the monoclinic cell. The character table and the basis vectors of the two IRs are given in Table 5.1(a,b). It is evident that the magnetic structure due to both the IRs will be noncollinear resulting from the superposition of ferromagnetic and antiferromagnetic components of the net moments.

Table 5.1(a): Character table and basis vector (magnetic) of space group Cc at ***k*** = 0,0,0

Irreducable Representation	Symmetry elements (Kovalve)	
	{1|0,0,0}	{σ|0.5,0,0}
Γ_1	1	1
Γ_2	1	-1

Irreducable Representation	Basis Vector		4a site	
			(x,y,z)	(x, -y, z+1/2)
Γ_1	$\tau_{3,1}$	Re Im	(1 0 0)	(-1 0 0)
	$\tau_{3,2}$	Re Im	(0 1 0)	(0 1 0)
	$\tau_{3,3}$	Re Im	(0 0 1)	(0 0 -1)
Γ_2	$\tau_{5,1}$	Re Im	(1 0 0)	(1 0 0)
	$\tau_{5,2}$	Re Im	(0 10)	(0 -1 0)
	$\tau_{5,3}$	Re Im	(0 0 1)	(0 0 1)

Table 5.1(b): Character table and basis vector (magnetic) of space group Cc at ***k*** = 0,0,1

Irreducable Representation	Symmetry elements (Kovalve)	
	$\{1\vert 0,0,0\}$	$\{\sigma\vert 0.5,0,0\}$
Γ_1^{001}	1	1
Γ_2^{001}	1	-1

Irreducable Representation	Basis Vector		4a site	
			(x,y,z)	(x, -y, z+1/2)
Γ_1	$\tau_{3,1}$	Re Im	(1 0 0)	(-1 0 0)
	$\tau_{3,2}$	Re Im	(0 1 0)	(0 1 0)
	$\tau_{3,3}$	Re Im	(0 0 1)	(0 0 -1)
Γ_2	$\tau_{5,1}$	Re Im	(1 0 0)	(1 0 0)
	$\tau_{5,2}$	Re Im	(0 10)	(0 -1 0)
	$\tau_{5,3}$	Re Im	(0 0 1)	(0 0 1)

5.4 Results and discussion

5.4.1 Room temperature Rietveld refinement of BF-0.25PT

Synchrotron x-ray powder diffraction (SXRD) patterns of 200,220, 222 and 400 reflections of BF-0.25PT for the sizes of ~ 150, 300, 500 and 2000 nm are given in Chapter III.In order to remove any ambiguity due to limited number of peaks in the SXRD pattern, we also used high resolution and higher "*q*" neutron diffraction data collected well above the Néel transition temperature T_N where no magnetic peak is present, for structure refinement. The results of Rietveld refinement of the nuclear structure at high temperature (750K) using neutron diffraction pattern is shown in fig. 5.1 for Cc (core)+Cc (shell), Cc (core)+R3c (shell) and Cc (core) + P4mm (shell)and R3c (core) + P4mm (shell) structural models. As in the case of SXRD data, we find that Rietveld refinement using neutron data also increases χ^2 for the two phase models with respect to that of the single phase refinement using Cc space group. This proves that the increase in χ^2 for two phase refinements is not due to limited number of peaks in SXRD patterns. This suggests that the system remains in the monoclinic Cc phase even after size reduction with insignificant contribution due to the disordered atoms, if any, in the shell region which cannot be captured by Rietveld technique.

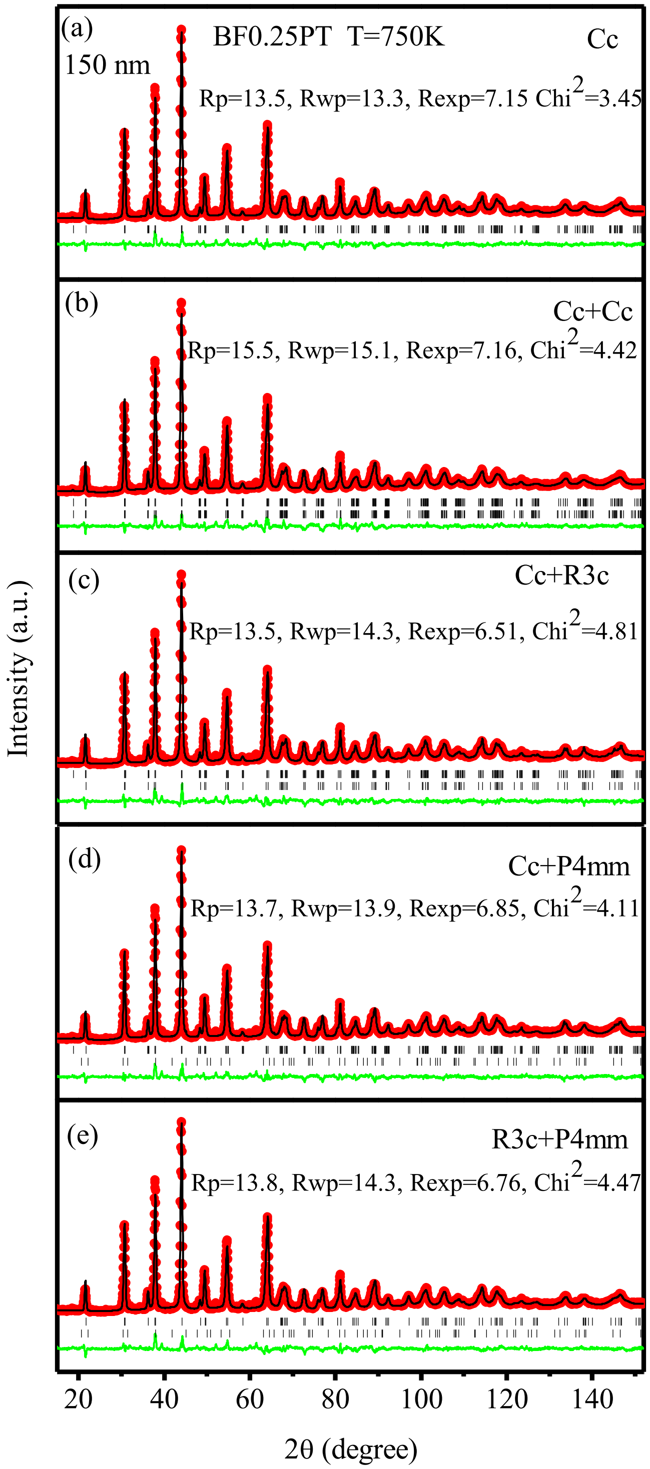

Fig. 5.1 Rietveld refinement profile for different structural models (a) Cc (b) Cc+Cc (c) Cc+R3c (d) Cc+P4mm and (e) R3c+P4mm of neutron powder diffraction pattern taken at 750K for 150nm size BF-0.25PT.

5.4.2 Magnetization studies of BF-0.25PT powder

The DC M(T) measurements were carried out at 500Oe from 300K to 900K.Fig.5.2 shows the M(T) plot for the samples with particle sizes 2µm, 500 nm, 300 nm and 150 nm. These plots clearly reveal a peak corresponding to the antiferromagnetic transition. The Néel transition temperature (T_N) was determined from the derivative plots of the M(T) curves in the vicinity of the peak temperature. The 2µm size powder, which we shall treat as representative of the bulk behavior shows T_N at 445K. Below the T_N, there is another transition, which is better revealed in the derivative plot (inset of fig 5.2a). This transition is known to be due to spin reorientation transition in bulk BF-0.25PT [Bhattacharjee et al .(2013)].

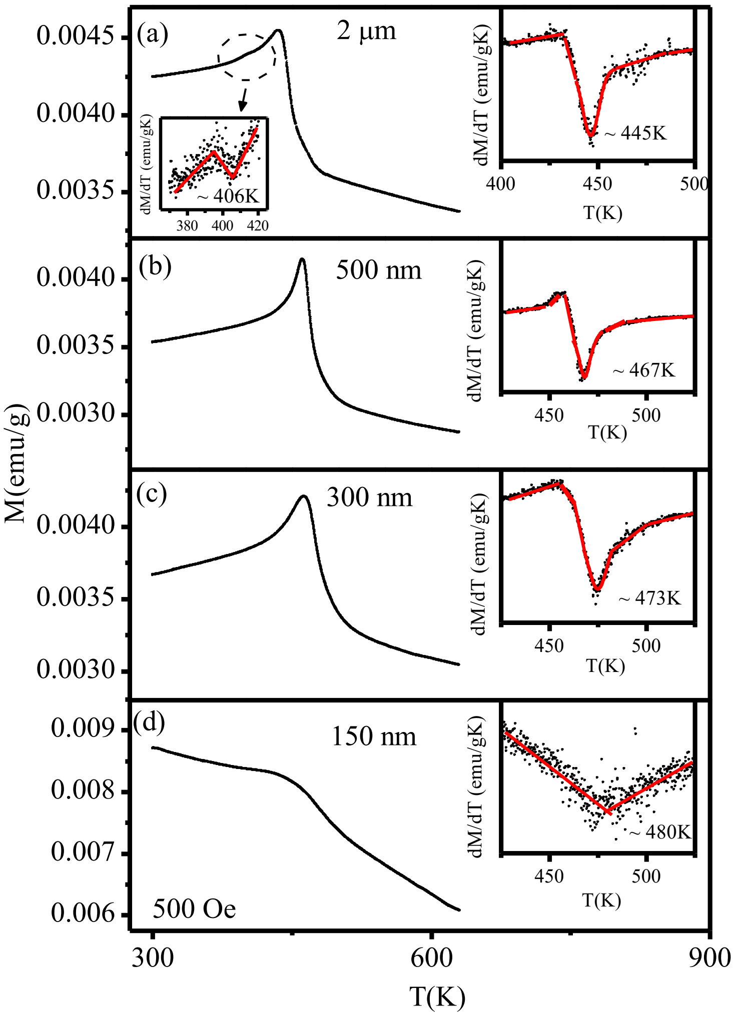

Fig. 5.2 Temperature dependence of field heating (FH) magnetization (M) for (a) 2μm (b) 500 nm (c) 300 nm and (d)150 nm BF-0.25PT sample.

On decreasing the particle size below 2μm, the signature of spin reorientation transition disappears. As a result, the AFM peak in the M(T) plot for 500 nm size powder becomes relatively sharper than that for 2μm powder (compare Fig 5.2 (a) and (b)). However, on decreasing the particle size further, the AFM transition peak shows rounding and smearing (see Fig. 5.2 (c) and (d)). The 150nm size powder infact shows very broad peak around T_N. This broadening is not induced by $PbTiO_3$disorder which is fixed at x=0.25

but is essentially a signature of the finite size effect [Binder et al. (1972)]. On decreasing particle size below 150 nm, the tetragonal phase starts appearing and hence our study of the finite size effect in the monoclinic phase was restricted upto 150nm size powders only. When the tetragonal and monoclinic phases coexist, the situation become more complex as these phases can also form a core -shell structure in the same particle. The most remarkable feature of the M(T) plots in Fig 5.2 is the increasing trend of T_N with decreasing particle size. This is in marked contrast to the situation in pure BF where on decreasing the particle size, T_N was shown to decreases as per the predictions of the Scaling theories [Lang et al. (2006)].

As the M(T) plot shows a rather broad peak around T_N for 150 nm size powder, the T_N was cross-checked using neutron scattering measurements also for this smallest size. Fig. 5.3(a) depicts the evolution of neutron diffraction pattern of the 150 nm size powder in a limited 2θ range for temperatures from 300 to 600K. The first peak at ½ ½ ½ pseudocubic position in these patterns, marked by an arrow, is the characteristic antiferromagnetic peak. The variation of the integrated intensity of this peak with temperature is depicted in fig.5.3(b). It is evident from this figure that the intensity of the antiferromagnetic peak decreases on increasing the temperature above 300K almost linearly. This is expected, as the intensity of the antiferromagnetic peak is proportional to the square of the order parameter. Above about 500K, the intensity follows a different slope with considerably reduced value. The remanent intensity above 500K is due to the presence of short-range antiferromagnetic correlations above T_N as well as the presence of a nuclear peak due to the Cc space group with rather low intensity. Most interestingly, the slope of the linear plot changes around 480K which corresponds to the T_N for the 150 nm size sample determined by M(T) measurements. This provides an independent confirmation of the transition temperature determined by M(T) measurements.

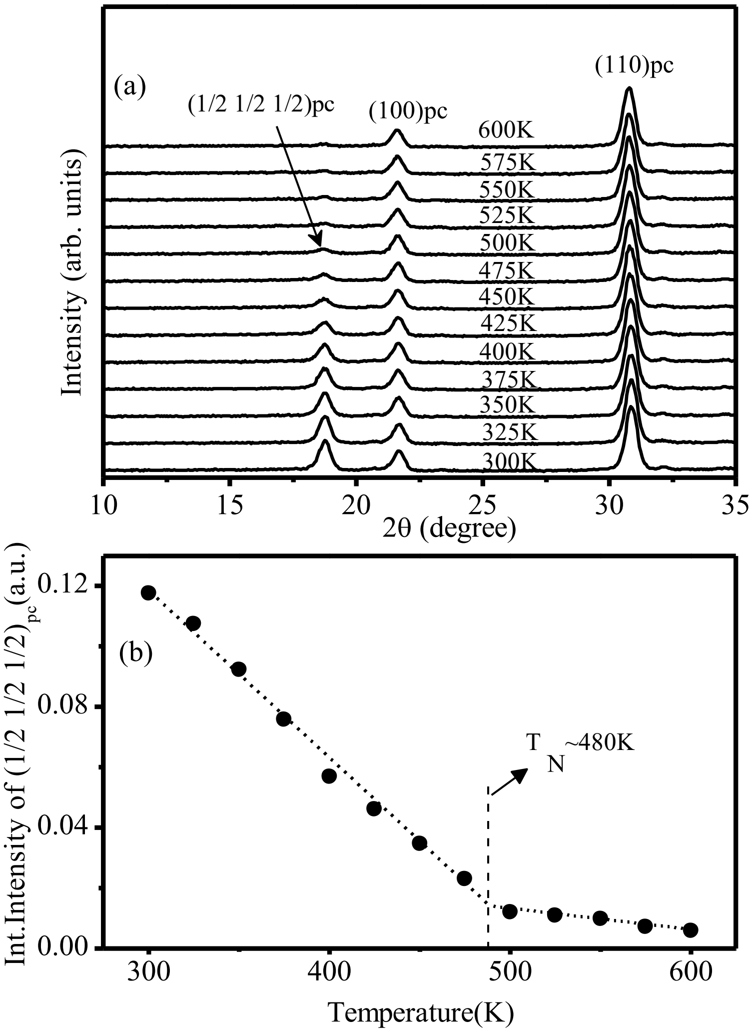

Fig. 5.3 (a) Temperature dependent neutron profile of BF-0.25PT in the low 2θ region (b) Integrated intensity of first magnetic peak of sample BF-0.25PT of size 150nm.

5.4.3 Effect of particle size on spin reorientation transition

The monoclinic compositions of BF-xPT have been shown to undergo a spin reorientation transition below the Néel temperature. The magnetic transitions have been described in the following manner by Bhattacharjeeet al (2013) with decreasing temperature:

Paramagnetic $\xrightarrow{T_{OPT}} \Gamma_2^{001}(G^y F^{xz}) \xrightarrow{T_N} \Gamma_1^{000}(G^{xz} F^y)$, where Γ_2^{001} and $\Gamma_1^{000}$are the irreducible representations (Irrep) of the magnetic Fe sublattice (4a Wyckoff site) forpropagation vectors k = 0,0,1 and 0,0,0 while G^yF^{xz}; $G^{xz}F^y$ present the magnetic structure in Bertaut notation corresponding to the two Irreps. In the Bertaut notation, G and F stand for AFM and FM components while the superscripts denote the direction (x/y) or plane (xz/xy) of magnetisation.

The M(T) plot for 2 μm sample reveals both the Néel temperature (T_N) and spin reorientation temperature (T_{OPT}) are 445 K and 406K, respectively (see Fig. 5.2(a). However, on decreasing the particle size, there is no evidence of the spin reorientation transitions in the M(T) plots. Since the reduction in particle size leads to the rounding and smearing of the AFM transition peak in M(T) (see Fig. 5.2(c) and (d)), it is likely that the weak anomaly at the spin reorientation temperature is getting masked by particle size broadening. In order to verify the presence or otherwise of the spin reorientation transition, we carried out Rietveld refinement of the magnetic structure using the neutron powder diffraction data at 450K, a temperature just below T_N but above the bulk spin reorientation transition temperature T_{OPT}, using all the possible Irreps, i.e. Γ_1^{001} and Γ_2^{001} belonging to k = 0,0,1 and Γ_1^{000} and Γ_2^{000} belonging to k=0,0,0 as discussed by Bhattacharjeeet al (2013). The results are shown in Fig. 5.4. The values of χ^2 and R_{mag} belonging to each model have been given in this figure. Evidently, the IrrepΓ_1^{000} gives the best fit amongst all the possible models indicating that the magnetic structure at this temperature belongs to the $\Gamma_1^{000}(G^{xz}F^y)$ Irrep.

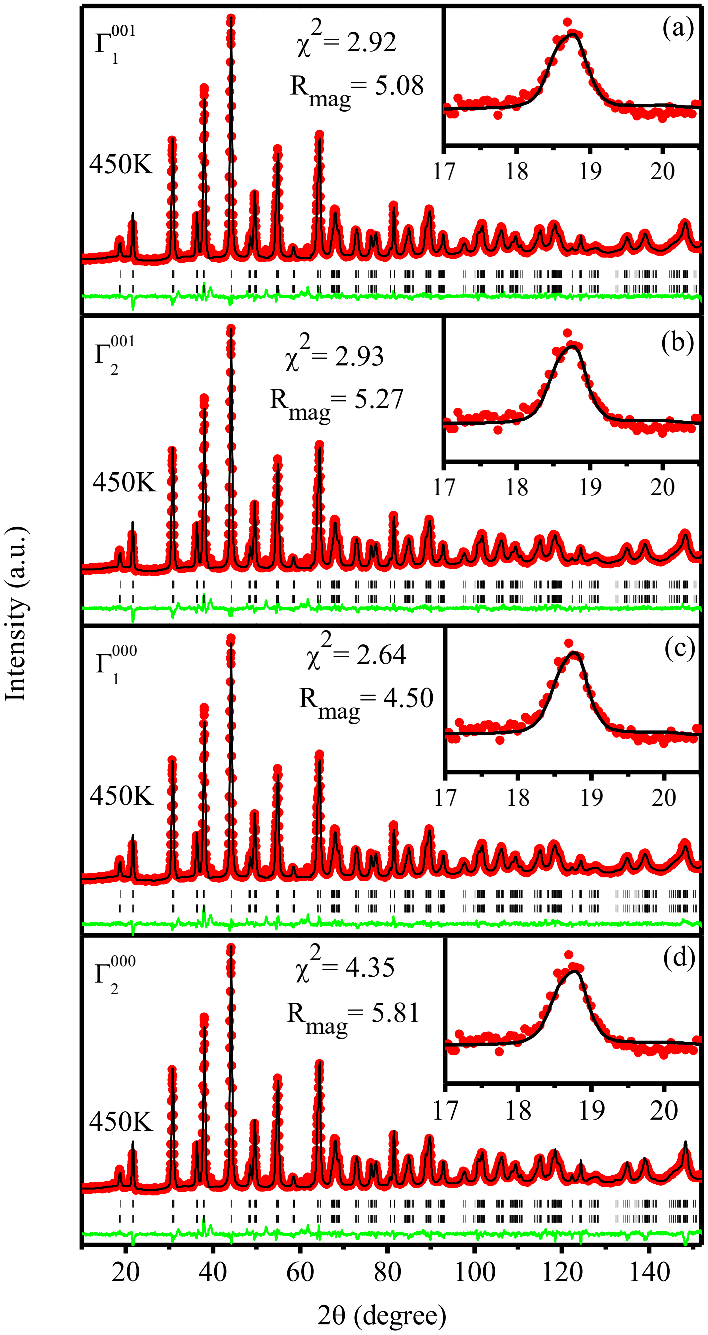

Fig. 5.4 Rietveld refinement of the magnetic structure using the neutron powder diffraction data at a temperature 450K using all the possible representations.

At room temperature (300K) also (i.e. below T_{OPT}), the Irrep Γ_1^{000} gives a better fit with lower χ^2 Bhattacharjee et al. (2013). The Irrep Γ_2^{000} leads to an inferior fit with higher χ^2. Figs. 5.5 (a) and (b) show the Rietveld fits for 150 nm sample at 300K using the Irreps Γ_1^{000} and Γ_2^{000}, respectively. The refined parameters obtained for 300 K and 450 K are given in table 5.2. On the basis of the refinements using neutron powder diffraction data, we may conclude that the spin reorientation transition does not occur in the nanoparticles, as indicated by M(T) plots also. This is another feature of size reduction in the monoclinic compositions of BF-xPT for x < 0.27. Thus,the nanoparticles having the size of 150 nm undergo paramagnetic to G type AFM ordering, with spin configuration belonging to the Irrep $\Gamma_1^{000}(G^{xz}F^{y})$, directly without the intermediate structure reported for bulk by Bhattacharjee et al. (2013).

We also analysed the temperature dependence of the orderedmagnetic moment per Fe atom. This is shown in fig. 5.6. It is evident from the figure that the ordered moment drops rapidly upto ~473K, but does not vanish completely until the temperature reaches 700K. The temperature dependence of the ordered moment was fitted to a power law, $\mu = \mu_0\ [(T_N - T)/T_N]^{\beta}$, which gives the value of β=0.346. This value differs from the β value (½) expected for the molecular field theory and Landau theory of second order phase transition. This value of β is close to the value of the critical exponent 1/3obtained for spin-wave theory and Callen decoupling Eibschütz et al. (1967), Patel et al. (2013) and has been reported in orthoferrites as well as BF solid solutions [Bhattacharjee et al. (2010)].

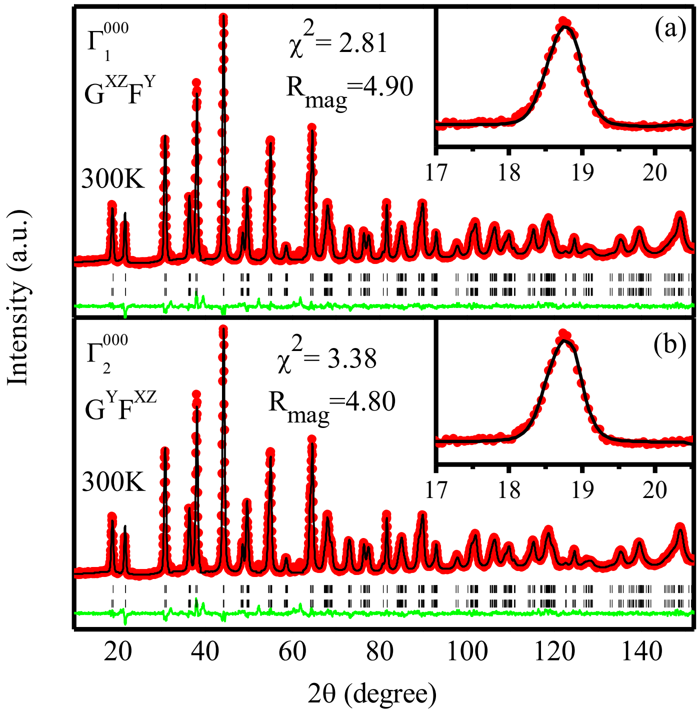

Fig. 5.5 Rietveld refinement of the magnetic structure using the neutron powder diffraction data at a temperature 300K using all the possible representations.

Table 5.2 Refined structural parameters of BF-0.25PTusing Cc space groupas obtained from neutron powder diffraction.

BF0.25PT ofsize 150 nm at different temp.		**Fractional coordinates**				**Thermal Parameters ($Å^2$)**	**Lattice Parameters (Å)**	**Statistical parameters**
		Atom	**x**	**y**	**z**			
300K	**Cc**	Bi/Pb	0.0	0.25	0.0	B_{iso}=1.12(3)	a=9.7846(1) b=5.5835(8) c= 5.6244(7) β = 125.66(5)	R_p= 7.72 R_{wp}= 8.91 R_{exp}= 5.31 χ^2 = 2.81 Magnetic R-factor: 4.9
		Fe/Ti	0.281(1)	0.256(4)	0.745(4)	B_{iso}=0.51(5)		
		O1	0.041(2)	0.306(9)	0.461(2)	B_{iso}=0.93(1)		
		O2	0.321(1)	0.489(6)	0.024(3)	B_{iso}=0.78(7)		
		O3	0.279(2)	-0.026(5)	-0.051(6)	B_{iso}=1.15(4)		
450K	**Cc**	Bi/Pb	0.0	0.25	0.0	B_{iso}=1.65(1)	a=9.8016(1) b=5.5928(2) c= 5.6294(3) β = 125.65(1)	R_p= 8.86 R_{wp}= 9.52 R_{exp}= 5.72 χ^2 = 2.64 Magnetic R-factor: 4.5
		Fe/Ti	0.280(1)	0.250(4)	0.744(7)	B_{iso}=0.84(1)		
		O1	0.039(8)	0.308(4)	0.458(1)	B_{iso}=1.21(1)		
		O2	0.317(1)	0.495(1)	0.018(6)	B_{iso}=1.21(6)		
		O3	0.276(4)	-0.021(7)	-0.048(6)	B_{iso}=1.59(1)		

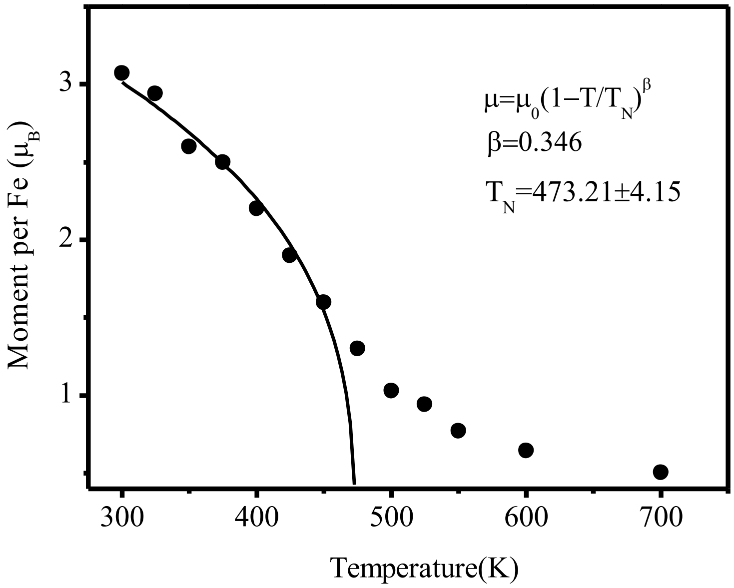

Fig.5.6 Magnetic moment (filled circles) obtained from the Rietveld refinements using the neutron powder diffraction data along with the fitted curve for $\mu = \mu_0\,[(T_N - T)/T_N]^\beta$.

5.4.4 Role of crystal-chemical parameters in enhancing T_N

The FE, FM and AFM transition temperatures (T_C) are known to decrease with decreasing particle size below a critical size. This decrease in transition temperature has been explained in terms of the scaling theories which relate the particle size (d) and the correlation length (ξ) with the T_C in the following manner [Binder et al. (1972).

$$\frac{T_C^b - T_C^{grain}}{T_C^b} = \left(\frac{d}{\xi_0}\right)^{-(1/\nu)} \qquad (5.1)$$

where T_C^b and T_C^{grain} are the bulk and finite size transition temperatures, *d* is the grain diameter, ξ_0 is the magnetic correlation length at 0K and ν the critical exponent related to ξ.

Thus, any increase in T_N with decreasing particle size is rather unusual and calls for an explanation. We had earlier shown a huge enhancement of T_N as a result of particle size reduction in a tetragonal composition of BF-xPT taking x=0.50 (BF-0.50PT) as example.

In case of BF-0.50PT nanoparticles, there is an increase in the Néel temperature from 120K for bulk to 350K for18 nm size particles. The increase in case of monoclinic BF-0.25PT is rather modest(T_N~445K for bulk to 480K for150 nm size particles). This difference in increase in T_N with decreasing size in tetragonal and monoclinic compositions also calls for an explanation. The huge enhancement of T_N in tetragonal BF-xPT was explained by us in terms of the reduction in the ferroelectric distortion leading to shortening of the longer Fe-O bond length along the [001] direction. As a result of such a shortening of the longer Fe-O bond length, the strength of the superexchange interaction increases leading to an increases of the T_N (discussed in chapter IV). This longer Fe-O bond length is much larger than the sum of the ionic radii of Fe^{3+} and O^{2-} as a result of which the superexchange interaction pathways are along [001] are nearly broken and AFM state of BF-0.50PT in bulk is essentially 2-dimensional (2d). Thus, the increase in T_N with decreasing particle size in the tetragonal phase of BF-xPT is essentially linked with a crossover from nearly 2d AFM ordering in bulk due to broken super exchange pathways in the [001] direction to a 3d AFM ordering in smaller particles due to reestablishment of superexchange interactions in this direction as a result of the reduced ferroelectric distortion. However, in the monoclinic composition of BF-0.25PT, none of the bonds is actually too large like BF-0.50PT and as such the exchange pathways are not completely broken. What is even more intriguing in case of BF-0.25PT is that the particle size dependence of T_N in this system is opposite to that of pure BF. In pure BF, T_N decreases with particle size as per the scaling law of Eq (5.1). [Selbach et al.(2007)]

To understand the effect of particle size on T_N in BF-0.25PT, we first present a comparison of the various Fe-O bond lengths, which decide the exchange pathways, for the bulk and nanocrystalline monoclinicBF-0.25PT, as well as and bulk rhombohedral BF as shown in Fig. 5.7(a) and (b).

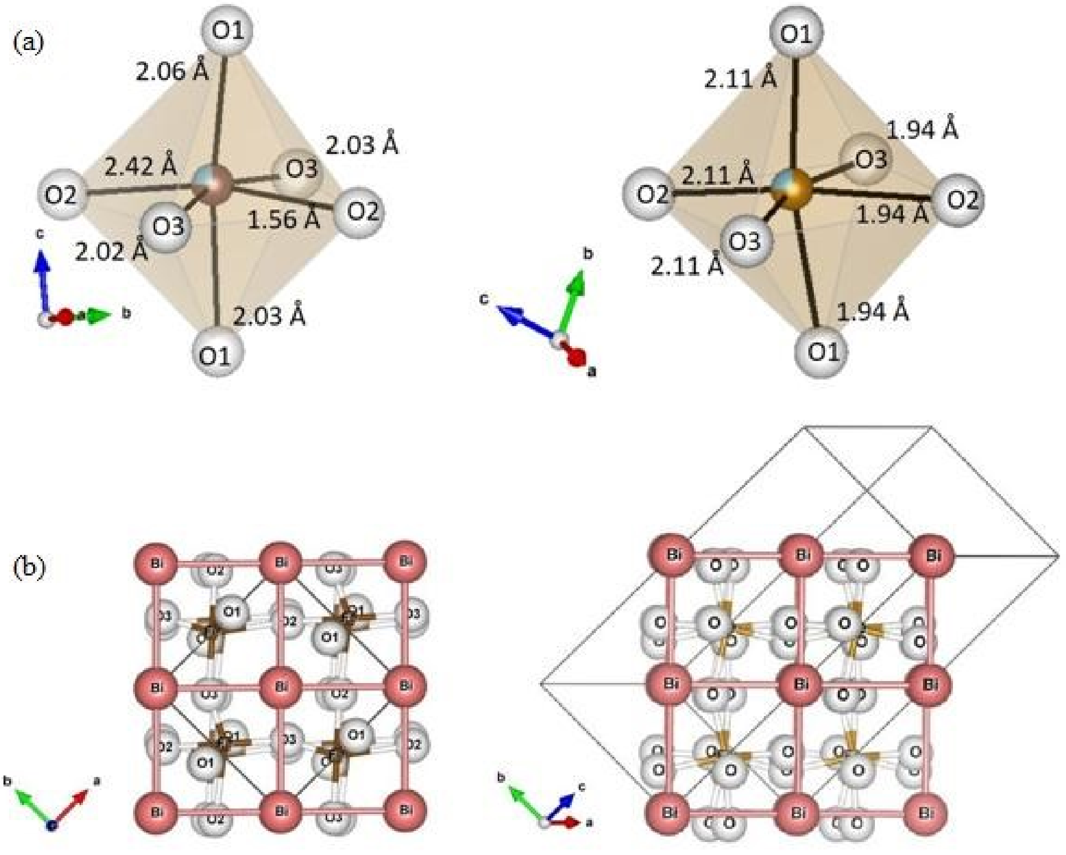

Fig. 5.7 (a) The Fe-O bond lengths for the octahedral coordination in monoclinic BF-0.25PT and rhombohedral $BiFeO_3$. (b) Comparison of asymmetry of bond lengths for BF-0.25PT and $BiFeO_3$.

The structural parameters obtained from Rietveld analysis of the SXRD were used to calculate the bond lengths and bond angles for Fe-O linkages belonging to the oxygen octahedron. The parameters so obtained are listed in Table 5.3. In the ideal perovskite structure, all the Fe-O bonds of the octahedron are equal and O-Fe-O bond angles are 180^0. As a result of ferroelectric distortion, one observes unequal Fe-O bond lengths and deviation from 180^0 bond angle. Corresponding to the three oxygen atoms, O1, O3 (both planar oxygen) and O2 (apex oxygen), in the asymmetric unit, there are three pairs of Fe-O bond lengths and three O-Fe-O angles different from 180°. The results of Rietveld refinement reveal a systematic change in the bond angles and bond lengths of the apex oxygen atoms. We define an asymmetry parameter as a measure of the deviation in the bond length from the ideal perovskite oxygen octahedra as a ratio of the difference in the two opposite bond lengths to the sum of these opposite bond lengths as given below

$$\text{\% Asymmetry (Asym)} = \frac{((Fe-O)_I-(Fe-O)_{II})}{((Fe-O)_I+(Fe-O)_{II})} X100$$

Table 5.3 Details of bond length and bond angle of BF-0.25PT of different sizes and bulk $BiFeO_3$ [Goswami et al (2011)].

Size (nm)	**Bond length (Å)**		**Asym (%)**	**Bond length (Å)**		**Asym (%)**	**Bond length (Å)**		**Asym (%)**	**Bond Angle (°)**		
BF-.25PT	$(Fe\text{-}O1)_I$	$(Fe\text{-}O1)_{II}$		$(Fe\text{-}O2)_I$	$(Fe\text{-}O2)_{II}$		$(Fe\text{-}O3)_I$	$(Fe\text{-}O3)_{II}$		O1-Fe-O1	O2-Fe-O2	O3-Fe-O3
2000	2.06(5)	2.03(5)	0.73	2.42(5)	1.56(5)	21	2.02(5)	2.03 (5)	~0	163.1(5)	151.4 (6)	166.5 (7)
500	2.13(5)	1.96(5)	4.15	2.37(5)	1.48(5)	23	2.07(5)	2.08 (3)	~0	162.0(6)	149.1 (7)	159.0 (6)
300	2.16(5)	1.94(5)	5.36	2.37(5)	1.49(4)	23	2.07(5)	2.09 (4)	~0	160.3(5)	146.3 (7)	157.8 (6)
150	2.21(5)	1.89(3)	7.80	2.47(6)	1.63(3)	21	2.01(7)	1.96(3)	~0	160.4(1)	146.2(5)	155.3(4)
Bulk $BiFeO_3$	2.11(8)	1.94(9)	4.15	2.11(8)	1.94(9)	4.15	2.11(8)	1.94(9)	4.15	167.4(1)	167.4(3)	167.4(2)

It can be seen from Table 5.3 that the asymmetry parameter significantly increases for the Fe-O1-Fe bonds from0.73 for bulk to 7.8% for the nanocrystalline sample, while the asymmetry for the Fe-O2-Fe bonds increases from 21% to 23% only. The Fe-O3-Fe bond lengths remain nearly symmetric and unaffected by particle size reduction. The systematic increase in the asymmetry parameter on decreasing the particle size correlates well with the Néel temperature of the samples which increases from 445K for bulk to

480Kfor 150 nm size particles (see Fig. 5.8). Further, the change in the asymmetry parameter is much more prominent between bulk and 500 nm size particles than between 500 nm and300 nm particles. This is consistent with the change in the T_N which changes from445K for bulk to 467K for the 500 nm size powders and thenfrom473Kfor 300 nm size to 480 K for 150 nm.

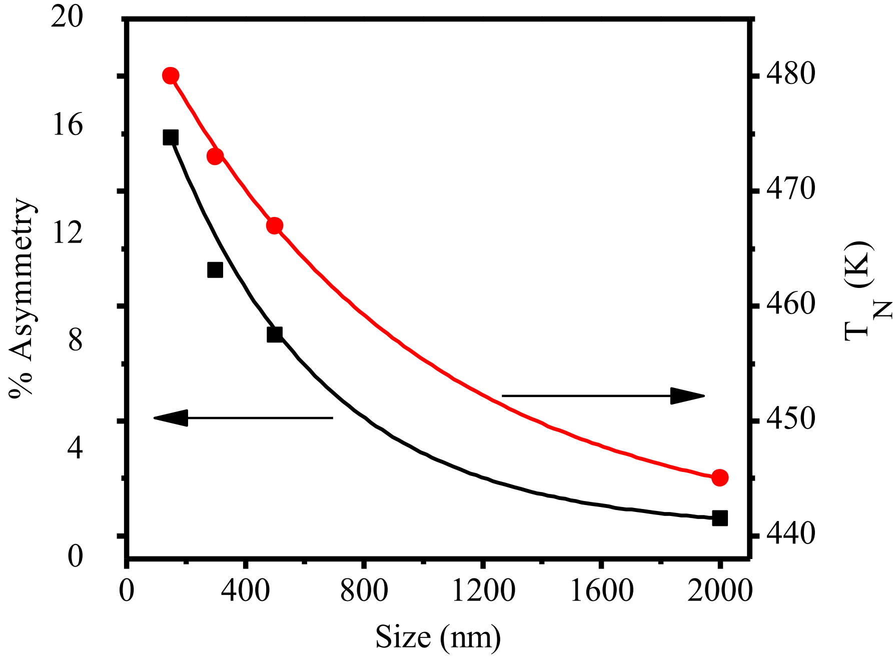

Fig.5.8 Variation of Neel temperature and percentage anisotropy with particle size of BF-0.25PT, highlighting their correlations.

The next question that arises is about the difference in the variation of the Néel temperature with particle size in rhombohedral $BiFeO_3$and monoclinic BF-0.25PT. While T_N of $BiFeO_3$follows the scaling theory [Selbach et al.(2007)], BF-0.25PT does not. The answer lies again in the structural details. In case of $BiFeO_3$, all the three Fe-O-Fe exchange pathways are equally asymmetric (see Table 5.3) for both bulk and nanocrystalline samples due to the rhombohedral space group R3c [Goswami et al. (2011)]. In contrast, in BF-0.25PT, the asymmetry parameter for the Fe-O1-Fe path way increases significantly with decreasing particle size and correlates well with the Néel temperature (see Fig. 5.9). Further, there is only a small variation in the asymmetry parameter for Fe-O2-Fewith size while asymmetry parameter is nearly constant for Fe-O3-Fe. Thus, the bond asymmetry parameter captures the most significant difference between BF-0.25PT and $BiFeO_3$for the three super exchange pathways. This difference is depicted in Fig. 5.6(b) at the elementary perovskite unit cell level. The uniform asymmetry along all the three superexchange pathways can be clearly seen in case of $BiFeO_3$in the figure but not in case of BF-0.25PT. It is very likely that these differences in the asymmetry parameter trigger a unique behavior in the nanoparticles of BF-0.25PT solid solution.

As mentioned earlier, the increase in the Néel temperature is quite large in case of BF-0.50PT, 120K for bulk to 350K for 18 nm size particles, whereas it is comparatively much smaller for BF-0.25PT. The major difference in the Fe-O-Fe superexchange pathways of tetragonal BF-0.50PT, monoclinic BF-0.25PT and rhombohedral $BiFeO_3$ is highlighted in Fig.5.9. In case of BF-0.50PT,one of the Fe-O1 bond lengths in the z direction is significantly larger than the sum of the two ionic radii due to the ferroelectric distortion. As a result, the exchange pathway is broken in the z-direction and the nature of AFM ordering becomes essentially 2-d. When the size is reduced, the ferroelectric distortion also decreases which in turn reduces the longer Fe-O bond length in the z direction. With decreasing Fe-O bond length, the superexchange interactions grow along the z direction leading to a cross over from 2-d to 3-d AFM interactions and increase in T_N. In case of BF-0.50PT, there is considerable room for this manipulation of the Fe-O bond length along the z-direction and hence the strength of the superexchange interaction.

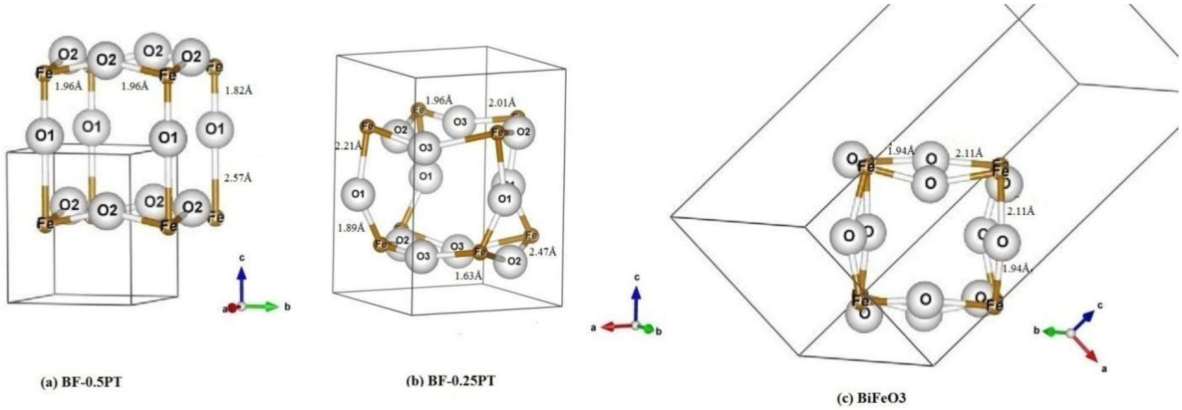

(a) BF-0.5PT

(b) BF-0.25PT

(c) BiFeO3

Fig.5.9 Fe-O-Fe exchange pathways (a) tetragonal $BiFeO_3$-0.50$PbTiO_3$, (b) monoclinic $BiFeO_3$-0.25$PbTiO_3$ and (c) rhombohedral $BiFeO_3$

This explains the large increase in the Néel temperature from 120K for bulk to 350 K for 18nm particles. In case of monoclinic BF-0.25PT, the Fe-O bonds are never broken in any direction due to the ferroelectric distortion and as a result there is comparatively much smaller change in the bond lengths due to size reduction. The superexchange pathways are already in the 3-d regime leaving less scope for manipulating the strength of the superexchange interactions through reduction in ferroelectric distortion with decreasing particle size. As discussed earlier, the increase in the asymmetry of the two Fe-O1 bond lengths with decreasing size in a particular direction seems to be playing the most significant role in deciding the strength of the superexchange interactions in case of BF-0.25PT. The asymmetry in the Fe-O bond lengths in case of $BiFeO_3$ is same in all the crystallographic directions irrespective of the size due to the rhombohedral symmetry in contrast to the previous two cases with tetragonal and monoclinic.

In Anderson's theory of superexchange interactions, the strength and nature of the interaction mainly depends on the overlapping integral of the participating ions, which in turn depends on the crystal field parameters Anderson (1950). So, in case of oxides where the magnetic ordering is getting facilitated through superexchange interactions, two physical parameters play very important role: the bond lengths in Fe-O-Fe and Fe-O-Fe bond angle. In case of tetragonal BF-0.50PT, only the bond length in c direction is affected by particle size, whereas size reduction strongly affects both the bond length and bond angle (see Table 5.3)in monoclinic BF-0.25PT.For such asymmetric superexchange interactions, an additional term $H_{DM} = D_{ij} \cdot (S_i \times S_j)$, where $D_{ij}$is the Dzyaloshinskii vector, needs to be considered in the main Hamiltonion Moriya (1960). For large asymmetries, the Dzyaloshinskii-Moriya(DM) interaction term cannot be ignored. We believe that it is this DM interaction term that may be responsible for increase in T_N with decreasing particle size in case of monoclinic BF-0.25PT.

5.5 Summary and conclusions

1. The Néel transition temperature (T_N) of BF-0.25PT increases from 445K for bulk to 480 K for 150 nm particle size using magnetization and neutron powder diffraction data. Based on Rietveld refined structural parameters, we show that the asymmetry and non-linearity of the Fe-O-Fe superexchange pathways grows with decreasing particle size and that they exhibit a strong correlation with T_N. We believe that thesubstantially enhanced Dzyaloshinskii-Moriya (DM) interaction with decreasing particle size as a result of asymmetric and non-collinear Fe-O-Fe superexchange pathways may be the key factor in raising the T_N on decreasing the particle size.

2. It has been established that the spin reorientation transition occurring below T_N in bulk monoclinic compositions like BF-0.25PT is suppressed in the nanocrystalline samples of ~150 nm particle size.

As it can be seen from the variation of integrated intensity of $(½,½,½)_{pc}$ peak with temperature shown in figure 5.3 and the variation of magnetic moment with temperature as shown in figure 5.6, there is a non-zero value persists even at temperature above the Neel transition temperature. We have investigated this peculiar behaviour as described in the chapter VI.

.